Renewable and Sustainable Energy Reviews 56 (2016) 851–864

Contents lists available at ScienceDirect

Renewable and Sustainable Energy Reviews

journal homepage: www.elsevier.com/locate/rser

The characterisation of the hydrodynamic loads on tidal turbines due to turbulence

I.A. Milne [a,*], A.H. Day [b], R.N. Sharma [a], R.G.J. Flay [a]

[a] Department of Mechanical Engineering, The University of Auckland, Private Bag 92019, Auckland Mail Centre, Auckland 1142, New Zealand
[b] Department of Naval Architecture and Marine Engineering, University of Strathclyde, Henry Dyer Building, 100 Montrose Street, Glasgow G4 0LZ, UK

ARTICLE INFO

Article history:
Received 5 March 2015
Received in revised form
21 November 2015
Accepted 30 November 2015

Keywords:
Tidal turbine
Turbulence
Unsteady hydrodynamics
Model-scale testing

ABSTRACT

An improved characterisation of the hydrodynamic blade loads due to onset turbulence is essential in order to mitigate premature failures, reduce excessive levels of conservativeness and ultimately ensure the commercial viability of tidal turbines. The literature focussing on the turbulence in fast flowing tidal streams and of the unsteady loads that are subsequently imparted to rotors has previously been very limited. However, increased activity in the tidal energy community has led to new investigations and insights which are reported in this paper.

It has been found that through the use of acoustic Doppler-based sensors, the streamwise turbulence intensities generally tend to a value of approximately 6–8% at the mid-depth of proposed tidal energy sites. Evidence that the anisotropic structure and scales of the turbulence are more consistent with open-channel-based models than atmospheric-based correlations has also been found. Rapid distortion theory has been applied to estimate that the standard deviation of the streamwise turbulent velocity fluctuations in the onset free-stream flow may be amplified significantly by 15% due to the presence of a turbine. The turbulent fluctuations have also been predicted to remain well correlated over the outer span of the blades at the rotational frequency of the rotor.

Recent model-scale experiments have enabled the unsteady hydrodynamic loading to be isolated from the steady-flow loading. For cases where the boundary layer remains primarily attached across the blades, this has enabled linear transfer functions to be developed and applied to model the response to a multi-frequency forcing. It has also been found that phenomena consistent with delayed separation and dynamic stall can result in a blade root bending moment that exceeds the steady value by 25%, and this needs to be taken into account in design to reduce the probability of failure.

Contents

* Corresponding author. Tel.: +64 9 373 7599x88146; fax: +64 9 373 7479.
E-mail addresses: imil015@aucklanduni.ac.nz (I.A. Milne), sandy.day@strath.ac.uk (A.H. Day), r.sharma@auckland.ac.nz (R.N. Sharma), r.flay@auckland.ac.nz (R.G.J. Flay).

http://dx.doi.org/10.1016/j.rser.2015.11.095
1364-0321/

1. Introduction

If tidal stream energy is to be competitive with other forms of energy generation, tidal turbines must be economical to manufacture and operate reliably over their design life of at least 20 years [1,2]. Reliability is particularly critical for turbines which are deployed in more remote communities. In these locations, replacement components and expertise are not likely to be readily available and electricity supply would be jeopardized by failure [3]. This is however complicated by the harsh and unforgiving environment in which tidal turbines must operate.

There are now several examples of early-generation turbines that have experienced catastrophic failures. This has been attributed to underestimating the magnitudes and the spectral characteristics of the hydrodynamic loads [4]. Furthermore, only draft industrial guidelines exist for accounting for both the turbulence and unsteady loads on tidal turbines [1]. These guidelines incorporate empirical models and theories that were devised primarily for wind turbines and which have not been extensively validated for tidal turbines. In an attempt to mitigate potential failure, designers of tidal turbines have resorted to incorporating excessive safety factors in fatigue load predictions which has subsequently increased the cost of the turbines [5,6].

In order to gain confidence in the predictions of the hydrodynamic loading, prevent unexpected failures and ultimately improve the economics of tidal turbines, the industry faces a number of significant issues and challenges. Firstly, compared to the mean flow, there is paucity of data available on the turbulence characteristics in strong tidal flows. This is indicative of the inherent technical difficulties in acquiring measurements of turbulence in fast flowing currents and the relative infancy of the tidal stream turbine industry [7]. Appropriate strategies to obtain measurements of the turbulent flow at tidal energy sites must therefore be devised. These should allow for not only the magnitudes of the turbulence to be observed, but also the structure and dominant scales which are crucial for informing the rotor loading [8].

It is also important to consider that the turbulence that is onset to a turbine and which induces the unsteady loading may differ to that which is observed in an undisturbed flow. In particular, the strain imparted on the flow field due to the extraction of momentum may distort the turbulence. Furthermore, a turbine blade rotates through a non-coherent turbulent field and may encounter an eddy multiple times. This can effectively give rise to a forcing spectrum dissimilar to that which would be measured at a fixed point. Therefore, appropriate techniques must be developed to quantify these effects in order to define the unsteady velocity that is incident on a rotor blade.

The unsteady loads which are subsequently induced from this turbulent flow comprise a complex interaction of both unsteady non-circulatory and circulatory effects, the latter commonly associated with dynamic inflow. For turbines operating near peak power, additional circulatory contributions from delayed separation and dynamic stall of the blades can also be present. Comprehensive discussions on these effects in the context of helicopter rotors and wind turbines are provided by Peters et al. [9] and Leishman [10], for instance. Together, these frequency dependent effects can give rise to overshoots in the load magnitudes over the equivalent value that would be measured in steady flow, as well as hysteresis in the response. Their significance may also be comparably greater for tidal turbines compared to wind turbines, due to the higher fluid-to-structural density ratio [11], reinforcing the need for their quantification.

While numerous studies have characterised the hydrodynamic loads on tidal turbines for steady flow (see, for instance, [12,13]), studies for unsteady flow conditions have been limited. Such test data are necessary to quantify the significance of the unsteady hydrodynamic loading contributions, verify numerical models and ultimately develop design guidelines to account for unsteadiness. The lack of test data on unsteady loading is arguably attributed to the substantial cost of using large, high quality facilities which are required to account for the effects of scaling and to reduce the effects of blockage. This calls for appropriate methodologies to be developed to enable the underlying hydrodynamic phenomena and their complex interactions to be quantified. Obtaining measurements of the out-of-plane (thrust-wise) hydrodynamic loading is of utmost importance as it is this component which typically governs the total structural loading on a horizontal-axis tidal turbine [14,15].

2. Objectives

Drawing on these challenges, the primary aim of this paper is to present and discuss recent advances that have been made on the characterisation of turbulence at tidal energy sites and the hydrodynamic loading on tidal turbines. The issues addressed in this review have drawn significant interest recently, spanning across both academia and industry and in many instances involving joint industry partnerships.

Specifically, the experimental techniques which have been adopted by researchers to measure turbulence are discussed and observations of turbulence in fast flowing tidal streams are collated. This is followed by a description of the application of theoretical models to account for the amplification and rotational sampling of the turbulent eddies necessary to obtain the forcing imposed on a turbine. Methodologies for experimentally testing tidal turbines in unsteady conditions at model-scale are then critically reviewed. Finally, the underlying unsteady hydrodynamic phenomena acting on a rotor are discussed in view of the recent experimental measurements that have become available.

3. Observations of turbulence at tidal energy sites

3.1. Measurement strategies

Experimental studies from circa 1960s provided initial insights into the characteristics of the turbulence in the seabed boundary layer of tidal flows. Grant et al. [7] utilised hot film and electrocurrent techniques to observe the turbulence spectra at high wavenumbers ($k_x = \pi f/U > 1$, where f is the temporal frequency

and U is the streamwise mean velocity) at the Discovery Passage in Canada. The study found strong evidence for an inertial subrange, as described by the Kolmogorov model [16], where the turbulence structure is expected to tend towards isotropic at higher frequencies. Subsequent measurements of turbulence reported by Heathershaw [17], Soulsby [18] and Gross and Nowell [19] also demonstrated that when the near-bed velocity wavenumber spectra were scaled using the distance from the bed z, the spectra collapsed to theoretical forms expected for boundary layer turbulence (as described by Townsend [20]).

Advances in instrumentation such as sensors which are based on acoustic Doppler techniques have facilitated a greater understanding of the structure of turbulence in tidal channels. Acoustic Doppler Current Profilers (ADCPs) and Acoustic Wave and Current (AWAC) profilers which acquire flow data along inclined acoustic beams are now widely utilised in the field. ADCPs were introduced in the 1980s and a brief historical account of their development is presented by Simpson et al. [21].

Due to the use of divergent beams and the nonhomogeneity of the turbulence across the beam spread, the instantaneous three-dimensional velocity cannot be reliably resolved using an ADCP or AWAC. However, as was originally shown by Lohrmann et al. [22] in the case of an ADCP with four opposing transducer beams, by assuming that the second-order statistical moments of velocity are homogeneous over the beam spread, and provided that the sensor tilt is small, first order estimates of the along-channel and across-channel Reynolds shear stresses ($-\sigma_{uw}$ and $-\sigma_{vw}$) can be obtained by subtracting the variances of opposing beam velocities. The Cartesian variances ($\sigma_u{}^2$ etc.) can also be obtained through the summation of opposing beam variances, though this necessitates an independent measure of the turbulence anisotropy.

These variance-based techniques have proved popular (see for instance Stacey et al. [23], Osalusi et al. [24], Milne [25] and Bouferrouk et al. [26]) and have enabled new observations of these key turbulence parameters through the water column at tidal energy sites. However, the uncertainty analysis presented by Lu and Lueck [27] reinforced the importance of acquiring measurements from a rigidly mounted ADCP for the application of the variance technique in strong flows. This is because second-order terms which involve the sensor tilt must be neglected in an estimate of the stresses.

Acoustic Doppler Velocimeters (ADVs) were introduced in the 1990s (see Lohrmann et al. [28]). The three-dimensional point measurements of velocity that they can provide are arguably more suitable for analysing the turbulence properties of interest for tidal turbines than ADCPs. The sampling rates are also typically higher and the sampling volume is of the order of only 1 cubic centimetre. Therefore, this generally enables the turbulence spectrum to be resolved at the eddy producing scales and up to those which correspond to the low-wavenumber end of the inertial sub-range. However, the maximum wavenumber can be limited by the Doppler noise, which is more pronounced for the horizontal components relative to the vertical velocity component or the Reynolds stresses [29].

There are several studies which have utilised ADVs to acquire measurements of velocity variances, Reynolds shear stresses and turbulence spectra in natural tidal flows with mean velocities over a tidal cycle of less than 1 ms^{-1}; see, e.g. Kim et al. [30], Sherwood et al. [31], Trevethan [32] and Walter et al. [33]. ADVs have also recently begun to be applied to energetic tidal energy sites where the mean velocity is of the order of 2 ms^{-1}, typically necessary for commercial scale energy generation (see, for instance, [34,35,8]). However, for fast tidal flows, the technical difficulty in rigidly supporting the sensor generally limits their use to the acquisition of measurements relatively close to the seabed.

Drawing on the respective advantages of ADVs and ADCPs (or AWACs), it is desirable to quantify the turbulence at proposed tidal energy sites by acquiring data from both types of sensors located together at the seabed. This methodology was adapted in the study reported by Thomson et al. [34] at Puget Sound in Washington, where the ADV was positioned at an elevation of 4.5 m in a $h = 20$ m water depth and colocated with an ADCP and AWAC. Milne et al. [35,25] also analysed data acquired from a similar setup at the Sound of Islay in the Inner Hebrides of Scotland. This is a relatively narrow channel that is approximately 5 km long, 800 m wide and 50 m deep at the location of the instrumentation. The water level variation between flood and ebb at spring tide is also relatively small at approximately 1 m. The ADV was positioned at an elevation of 4.5 m, which was within an approximately logarithmic mean velocity profile region.

A key advantage of using an ADV together with an ADCP is that it can provide an independent estimate of the Reynolds stresses and turbulence intensities for verification purposes. This has been demonstrated recently by Milne [25] where good agreement was found between the two measurements at the Sound of Islay, with differences of 5% or less. A direct measure of the anisotropy also reduces the uncertainty in the application of the variance method to an ADCP with four transducers when estimating the turbulence intensities, where this parameter is otherwise unknown.

3.2. Magnitudes and structure of turbulence

The streamwise turbulence intensity ($I_u = \sigma_u/U$) is generally regarded as the turbulence parameter most relevant to the unsteady loading on tidal turbines [1,36,37]. It provides a quantification of the turbulent kinetic energy present in the flow, in a direction in which the angle of attack of the turbine blade is generally most sensitive. It follows that quantifying this parameter has been the focus of the majority of recent measurement campaigns at proposed tidal energy sites. These studies have provided valuable new observations of the turbulence intensity at various elevations from the seabed in relatively fast flows for a variety of channel configurations.

Observations of the streamwise turbulence intensity at an elevation of $z/h = 0.2$ from the seabed from ADV data at Puget Sound were reported by Thomson et al. [34] and McCaffrey et al. [8]. At peak flows of approximately $U = 1.5$ ms^{-1} the intensities varied between $I_u = 0.07$ and 0.10 and had a median value of $I_u = 0.084$. Measurements of the intensity in the flow at the operating SeaGen tidal energy site at Strangford Loch were presented by MacEnri et al. [38]. These were acquired at an elevation corresponding to the hub height of the rotor using an electromagnetic current meter (given that the streamwise intensity only was of primary interest in their study). The intensities tended to values of between $I_u = 0.05$ and 0.06 at peak flows of around 3.5 ms^{-1}. A recent ADV-based campaign reported by Gunawan et al. [39] provided observations at approximately the centre of the water column in the East River in New York. They found higher intensity values of $I_u = 0.13$ in a peak flood flow of 2.4 ms^{-1} and $I_u = 0.18$ in a peak ebb flow of 1.6 ms^{-1}.

Time-histories of the intensities relatively close to the seabed at an elevation of $z/h = 0.1$ at the Sound of Islay over two complete spring tidal cycles were presented by Milne et al. [35]. These are in Fig. 1 which shows that the intensity tended to median values of $I_u = 0.11$ and 0.13 at peak flood and ebb flow respectively. However, these time histories also importantly serve to elucidate the characteristics of the largest values of the intensities. Intensities of up to $I_u = 0.16$ were experienced over relatively short periods which were also associated with corresponding peaks in Reynolds stresses (a proxy relevant for quantifying the coherent energy). Given this, these instances of high intensities could be expected to

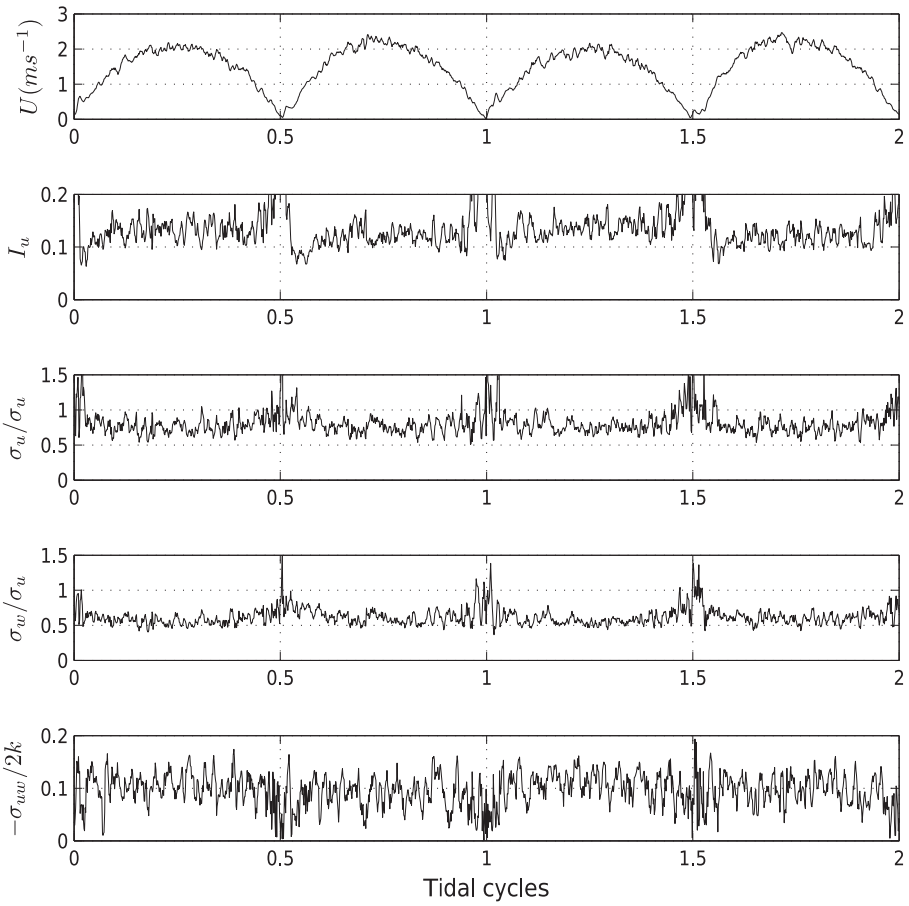

Fig. 1. Time histories of the 5-min average mean velocity, turbulence intensity, anisotropic ratios and ratio of the Reynolds stress to twice the total kinetic energy at the Sound of Islay observed during spring tide [25].

Table 1
Summary of turbulence properties (median values) observed in tidal channels, open-channel flows in the laboratory and in the atmospheric boundary layer.

Location	I_u (peak flow)	σ_v/σ_u	σ_w/σ_u	$-\sigma_{uw}/2k$
Puget Sound ($z/h=0.2$)	0.08	0.75	0.50	–
Strangford Loch ($z/h\approx0.5$)	0.05–0.06	–	–	–
Sound of Islay ($z/h=0.1$)	0.11 (flood), 0.13 (ebb)	0.70, 0.75	0.50, 0.55	0.09, 0.11
East River ($z/h\approx0.5$)	0.13 (flood), 0.18 (ebb)	–	–	–
Menai Strait ($z/h\leq0.2$)	–	–	0.63	0.09
Laboratory [46]	–	0.71	0.55	0.10–0.13
Atmosphere [45]	–	0.67	0.45	–

have a significant affect on the unsteady loading on a tidal turbine. This reinforces the fact that it is desirable for tidal turbine designers to obtain continuous samples of the turbulence to enable such events to be captured.

The median intensities at these aforementioned tidal energy sites are summarised in Table 1. However, to aid in the comparisons of the intensities between sites which were obtained at different elevations, Milne [25] also provided profiles of the 20-min average intensities throughout the water-column at the Sound of Islay. These were estimated from ADCP records and incorporated the anisotropic ratio estimated by the ADV. At the elevations of $z/h=0.2$ and $z/h=0.5$, corresponding to the observations by Thomson et al. [34] and MacEnri et al. [38], the intensities were approximately 0.08 and 0.07, respectively, which is in good agreement with their findings. In lieu of mean velocity profiles or frictional velocities being reported by Gunawan et al. [39], it is difficult to ascertain the underlying causes for the relatively high values observed at the East River compared to Puget Sound, Strangford Loch or the Sound of Islay. Is is perhaps possible that the channel geometry and the bedform may have given rise to significantly different flow conditions compared to these other sites. In view of studies such as by Blumberg and Pritchard [40], flow stratification in the East River may have also affected the flow. Nevertheless, these East River data serve to highlight the usefulness of acquiring physical measurements as they can reveal crucial site-specific characteristics.

Notwithstanding the importance of the streamwise intensity, additional second-order statistics are also of interest for inferring the turbulence structure of the onset flow and coherent eddies, as well as for developing simple turbulence models [8]. The Reynolds stress (referred in terms of the co-variance $-\sigma_{uw}$), for instance, provides a measure of the energy contained by the eddies involved with the turbulent mixing in the vertical direction. These stresses have been associated with coherent loading on rotors (see Sutherland [41]) and also peaks in the turbulence intensity as mentioned previously. Observations of the profiles of these stresses by Stacey et al. [23], Osalusi [42] and Milne [25] in tidal streams have shown that the variations in these stresses do often conform to an inverse proportion relationship with elevation from the bed predicted for open channel flows (see, for instance, Townsend [20]). However, the profiles reported by Osalusi [42] exhibited an unusually strong stress above the bed which was possibly related to the upstream topography. Furthermore, recent observations from a site in the Bristol Channel where the tidal energy was relatively low and there was significant wave action

reported by Bouferrouk et al. [26] also indicated that there were significant stresses in the upper water column. The authors suggest that these findings may be due to the action of waves breaking. Together these observations, in particular, serve as a poignant reminder that site-specific data are critical for assessing turbine loading.

From the ADV data set at the Sound of Islay, Milne [25] also presented ratios of the standard deviations of the lateral and vertical velocity fluctuations to that of the streamwise velocity fluctuations, as well as the ratio of the Reynolds stress $(-\sigma_{uw})$ to twice the total turbulent kinetic energy $(k=(\sigma_u^2+\sigma_v^2+\sigma_w^2)/2)$. The observations by Milne [25] are also presented in Fig. 1. The values of the ratios are shown to have remained relatively consistent during non-slack periods in the tidal cycle. Time histories of variances of the velocity fluctuations at the Puget Sound were also recently presented by McCaffrey et al. [8]. From these observations it can be deduced that the anisotropy also remained relatively constant with values of the ratios σ_v/σ_u and σ_w/σ_u within around 10% of those which were observed at the Sound of Islay. These ratios have seldom previously been provided for rapid tidal flows and the studies provided valuable new insights into the degree of the turbulence anisotropy that may be expected at a tidal energy site.

However, it is interesting to compare the observations at the Sound of Islay with reports for slower tidal channels and idealised flows which are summarised in Table 1. Interestingly, the ratios of σ_w/σ_u and $-\sigma_{uw}/2k$ compare relatively well (within 15%) with the ratios observed at the Menai Strait [17], which is a relatively narrow tidal channel with a flow speed of around 1 ms^{-1}. The ratios σ_v/σ_u, σ_w/σ_u and $-\sigma_{uw}/2k$ are also in excellent agreement (within 5%) with values for two-dimensional (i.e. width/depth >5) open channel flows in the laboratory. This suggests that the relatively simple correlations for idealised open channel flows may be applicable to such tidal energy sites similar in topography to the Sound of Islay or Puget Sound, and that the anisotropy may be relatively independent of the Reynolds number. Furthermore, these findings also suggest that the anisotropic ratios of $\sigma_v/\sigma_u=0.67$ and $\sigma_w/\sigma_u=0.45$ corresponding to the atmospheric boundary layer reported by Lumley and Panofsky [43] (and also listed in Table 1) are likely to be less applicable to tidal channels. The lower ratios observed in the atmosphere are consistent with the notion that energy in a tidal channel is restricted by the presence of a free surface, particularly in the vertical direction. Therefore, the use of atmospheric-based correlations in tidal turbine studies may lead to poorer estimates of the unsteady loading.

Finally, it is also useful to consider the use of other statistics which can provide meaningful insights into the turbulence structure and assist in developing models. For instance, in the analysis of the turbulence at Puget Sound, McCaffrey et al. [8] reported on the eigenvalues of the anisotropy tensor and the anisotropy magnitude, the latter which incorporates both coherent turbulent events and anisotropy. Using these metrics in their analysis, they found further support for the turbulence not being isotropic but rather primarily one and two-dimensional between the sampling frequency of 32 Hz and the 10-min window employed. The ratio of the Reynolds stress $-\sigma_{uw}$ to the turbulent kinetic energy is also of interest for verifying the applicability of turbulent kinetic energy-based closure for one-equation turbulence models [19]. These models relate the turbulent kinetic energy to the Reynolds stress, as opposed to the mean shear velocity which invokes a mixing length model. The near constant value of these ratios throughout the tidal cycle observed by Milne [25] and observed in the Menai Strait, as well as the good agreement between the value assumed by Bradshaw et al. [44] suggests that such models are likely to still be attractive for the tidal energy industry. This is despite their acknowledged shortcomings in not accounting appropriately for the distribution of length scales of the turbulence [45].

3.3. Scales of the turbulence

Quantifying the scales at which the turbulence is distributed at a tidal energy site is also crucial for inferring the unsteady loading on a turbine and verifying turbulence models. The integral length scales of turbulence, defined as the integral of the autocorrelation function (i.e. $L_i=U\int_0^{\tau=R(0)}R_{ii}(\tau)d\tau$), provide a quantification of the average size of the energy producing turbulence scales. Observations of integral-scales for fast flowing tidal sites in the literature are generally scarce. Milne et al. [35] reports that at the Sound of Islay the median streamwise length scales at an elevation of $z/h=0.1$ were approximately 10 m and 13 m during the flood and ebb respectively. McCaffrey et al. [8] have also found an average integral length-scale at an elevation of $z/h=0.2$ at the Puget Sound of 11.6 m. It is interesting to compare these values with predictions which could be obtained from the model $L_u=\sqrt{zh}$ proposed by Nezu and Nakagawa [46]. In the case of Puget Sound in particular, the difference is only 7%. Therefore, in-spite of its inherent assumptions associated with an idealised steady flow and a relatively smooth bed, the model could provide reasonable estimates of this important scale.

However, it is imperative to note that the energy-producing scales at the Sound of Islay and Pugent Sound both exhibited a relatively large degree of variability over the tidal cycle (up to 81 m at Puget Sound), which would not be accounted for using the previous simplistic model. The observations that the energy-producing eddies encompass a broad range of scales appears to be a characteristic of tidal channels in general; see for example Trevethan [32] and Walter et al. [33]. The largest integral scales which were observed were also associated with oscillations at length-scales several orders of magnitude greater than the channel depth. Given this finding, they are not expected to be due to the turbulence generated from the bed. As commented by Milne [25] and Thomson et al. [34], it is postulated that the low frequency perturbations reflect the unsteady nature of the mean velocity over the tidal cycle, or large meandering structures in the flow which are perhaps shed from upstream headlands.

The co-spectra at 5 m and 30 m above the seabed observed at the Sound of Islay also provided useful insights into the variation in the scales with elevation at a tidal energy site. These showed that the peak co-spectral density did not scale exactly with elevation above the bed, as observed for atmospheric turbulence [43]. In line with the differences found in the anisotropy between a tidal channel and the atmosphere, these results are consistent with the assumption of the free-surface having constrained the size of the eddies associated with the turbulent mixing and which would not be the case in the atmospheric boundary layer.

The form of the streamwise spectra at high wavenumbers is of interest for identifying the scales at which the turbulence tends towards being isotropic. Evidence for the inception of a near $k_x^{-5/3}$ behaviour at wavenumbers higher than $k_xz=$ 3–4 was observed from the ADV data at the Sound of Islay. This is consistent with that observed at Puget Sound [34] (which can be estimated as $k_xz=3.9$–5.9) and at the Pickering Passage [47]. Interestingly, the inception is also in general agreement with the theoretical predictions of $k_xz=4.5$ [48].

Together these observations provide support for the non-dimensional wavenumber at which the inertial subrange occurs being a universal property for fast flowing natural tidal streams. At elevations of $z/h=0.4$–0.5, this non-dimensional wavenumber corresponds to scales of the order of the rotor diameter at the Sound of Islay. Therefore, this would imply that the Kolmogorov model [16] could be employed to provide useful predictions of the turbulent fluctuations at scales relevant to a tidal turbine.

4. Description of the unsteady forcing applied to tidal turbines

4.1. Rotational sampling of turbulence

A description of the turbulence-induced forcing imposed on a turbine blade requires the consideration that during each revolution, the turbine blade rotates through a turbulence field that is not fully spatially coherent. This action can give rise to significant energy contributions at multiples of the rotational frequency of the rotor, and is a primary contributor to the fatigue of rotor blades [41].

The effect of this phenomenon on the out-of-plane bending moment may be quantified by considering the rotational cross-spectrum of the streamwise turbulence between two points on the blade. A theoretical expression for the cross-spectrum for a rotor blade ($S_u^o(r_1, r_2, n)$) (where r_1 and r_2 correspond to two points inward and outward along the blade and n is the frequency) has been presented by Burton et al. [49]. This was derived from the isotropic von Kármán spectrum and its corresponding correlation functions [50].

Milne et al. [35] found that the von Kármán spectrum provided a reasonable description of the streamwise velocity spectrum at the Sound of Islay at an elevation of $z/h = 0.1$. On this basis, by incorporating the observed integral length-scales of 11 m at this elevation with the theoretical correlations, useful insights into the spectra that would be observed by a typical full-scale tidal turbine blade were obtained by Milne [25] (assuming a tip-speed ratio of 5 and a blade length of 10 m). For instance, and referring to Fig. 2, at frequencies near the rotational frequency, the cross-correlation function of the turbulence is relatively high across the outer-blade sections. For a constant tip-speed ratio, the rotational sampling effect (i.e. the distortion of the spectrum) at very low frequencies reduces as the ratio r/L_u^x decreases. However, even for an integral-length scale of 42 m, which may be more realistic at the mid-depth at the Sound of Islay based on the correlations presented by Nezu and Nakagawa [46], the turbulent energy at the revolution frequency and the correlation of the turbulence across the outer blade sections remains relatively high for a typical tidal turbine rotor.

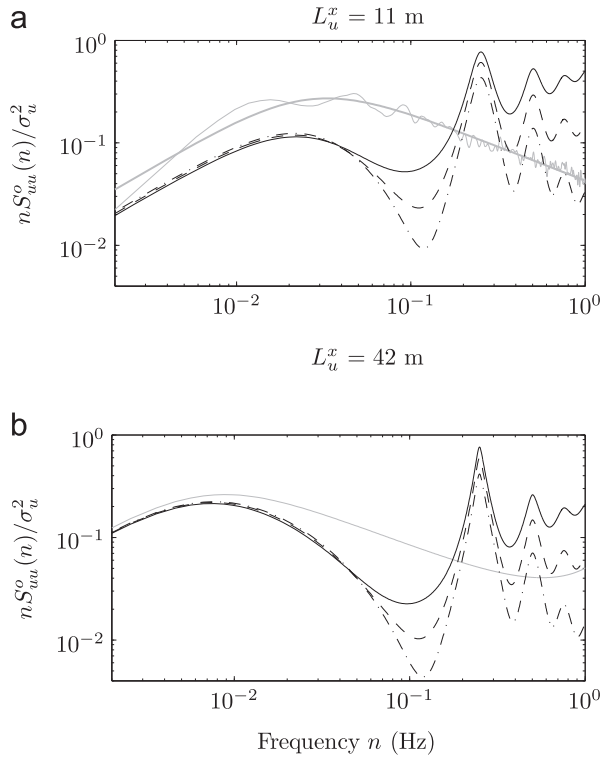

Fig. 2. Rotational sampled streamwise auto-spectral density observed at a point at $r=$ 10 m (solid black line) and the rotationally sampled cross-spectrum between points at $r_1=$ 10 m and $r_2=$ 6 m (– –) and $r_2=$ 4 m (-.-), assuming the integral-length scales of $L_u^x=$ 11 m, (a) and $L_u^x=$ 42 m, (b) as computed by Milne [25]. The model is derived from the von Kármán spectrum and assumes a tip-speed ratio of $\lambda = 5$. The corresponding auto-spectrum is shown in grey, with the observed spectrum at 5 m also shown in (a) in grey (bold).

As the total variance remains constant between the Eulerian and rotational systems [51], the turbulence intensity measured in the free-stream becomes concentrated at the rotational frequency. Therefore, the dominant frequencies of interest for quantifying the blade loads are expected to range from those corresponding to the integral scales, up to those which are equivalent to the rotor frequency (i.e. $n = 0.4$ Hz for the SeaGen rotor [52]). The effect of rotational sampling implies that the reduced frequencies ($k = \pi nc/\Omega r$) that would be applicable to tidal turbines due to turbulence are likely range between $0.02 < k \leq 0.10$.

An additional important consequence of the relatively high correlation across the blade length is that the forcing on a turbine blade could be replicated approximately in a laboratory by subjecting the rotor to oscillatory planar forcing. This is because the out-of-plane bending moment is dominated by the loading over a relatively small region at the outer-span of the blade. This result was used by Milne [25] as a justification for using planar oscillatory motion to experimentally measure the unsteady loading on tidal turbine blades.

4.2. Amplification of turbulent fluctuations

As a consequence of the turbulence scales in the onset flow not being significantly larger than typical rotor diameters, the strain field imparted on the mean flow by the presence of the rotor may also distort the vortices, contracting them axially and expanding them laterally. Batchelor [53] applied rapid distortion theory to show that the turbulent kinetic energy of a homogenous turbulent stream could be significantly attenuated when subjected to a constant strain in a wind tunnel contraction. A similar significant distortion of turbulence in a weakly-nonhomogenous flow at length scales smaller than the diameter of a porous plate was reported by Graham [54]. This situation may be analogous to the resistance imposed by a tidal turbine.

In a novel application of the rapid distortion theory-based solution presented by Batchelor [53], Milne [25] and McNae and Graham [55] have predicted the amplification of the velocity fluctuations due to an isolated tidal turbine extracting energy from the flow. The application of the linearised theory requires that the inertia and viscous forces can be neglected during the distortion, i.e. $\sigma_u/U \ll L_u/D$ (where D is the rotor diameter). This appears to be a reasonable assumption for tidal energy sites where $\sigma_u/U \approx 0.1$ and the ratio of the integral length-scale to the rotor diameter is of the order of 1. Furthermore, the solution presented by Batchelor [53] also assumes that the turbulence is isotropic. While the largest scales at a tidal energy site are not isotropic, at an elevation of $z/h \approx 0.5$ the momentum flux co-spectra at Islay indicated that the turbulence was tending towards isotropy at scales corresponding to the rotor diameter. On this basis, the rapid distortion model is still likely to provide a useful first-approximation of the amplification.

To demonstrate the approach, and referring to the schematic in Fig. 3(a), an estimate of the strain across the streamtube may be obtained from the expansion ratio $e = A_d/A = U/U_d = (1-a)^{-1}$ (where A is the area of the streamtube upstream, A_d is the area of the rotor, U and U_d are the streamwise mean velocities upstream and at the rotor, respectively, and a is the axial induction factor) and applying one-dimensional linear momentum theory to an actuator disk. As such, the velocities can be related through the axial induction factor; see e.g. Burton et al. [49]. For a turbine operating in optimal conditions the induction factor has a value of $a = 1/3$, which corresponds to an expansion ratio of $e =$ 1.5. As

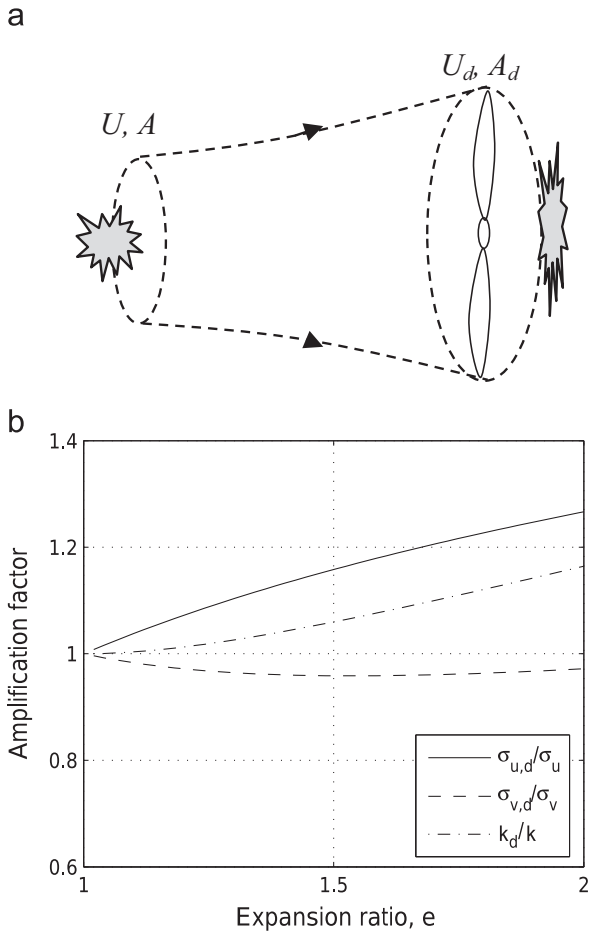

Fig. 3. A schematic of the streamtube whereby a strain is induced on the homogenous turbulence due to a reduction in the axial velocity, resulting in an axial contraction and lateral expansions of the vortices (a). Amplification of the standard deviation of streamwise velocity for a sudden expansion as a function of the expansion ratio, $e = A_d/A$ as predicted using Rapid Distortion theory and reproduced from Milne [25] (b). A typical turbine is expected to correspond to an expansion ratio of $e = 1.5$.

shown in Fig. 3(b), the amplification of the standard deviation of the streamwise velocity for an ideal turbine is approximately 15%. The corresponding spectra at the rotor were computed by McNae and Graham [55] using the von Kármán theoretical spectrum. This demonstrated that it is the energy of the largest eddies which are most affected by the presence of the rotor.

These analyses suggest the amplification effect is significant and reinforces the need to consider the effect of the turbine when inferring the unsteady loads from site data in an undisturbed flow. Based on the amplification effect, the ratio of the velocity amplitudes to the mean velocity relevant to tidal turbines due to turbulence is likely to be up to $\tilde{u}/U = 0.2$. However, it also important to note that the variation in the mean velocity with depth also induces a once-per-revolution forcing. As such, the Current numbers applicable to a full-scale turbine could be 50% larger than those due to turbulence alone [25].

5. Methodologies for quantifying the unsteady hydrodynamic loading on tidal turbines

5.1. Experimental techniques

Compared to full-scale, model-scale testing offers the advantage of a more controlled and less expensive means of investigating the hydrodynamic loads on tidal turbines that are likely to be induced by turbulent flow. A variety of techniques have been employed by investigators to acquire unsteady loading data for horizontal-axis tidal turbines at model-scale. These have helped to inform new test guidelines and procedures for tidal turbine testing [56]. Moreover, they have also highlighted additional challenges compared to steady flow -based tests.

Maganga et al. [57] and more recently Mycek et al. [58] investigated the sensitivity of the mean thrust of a 700 mm diameter (approximately 1/30th scale) tidal-turbine to a variation in the turbulence intensity in a flume, achieving intensities of between 3% and 25%. However, Maganga et al. [57] did not report the inlet scales which makes relating their results to full-scale inherently challenging. As discussed in International Towing Tank Committee (ITTC) guidelines [56], the use of advanced velocimetry techniques can enable the essential onset turbulent scales in flumes to be characterised. To this end, the spectra presented in the subsequent study at the same facility by Mycek et al. [58] indicated that the turbulent energy was primarily concentrated at frequencies less than 0.5 Hz. This corresponds to length-scales of 1.5 m or at least twice the diameter of the rotor that was used in the experiment. Based on the integral scales reported for tidal energy sites, these turbulence-to-rotor length-scale ratios could therefore be considered to be reasonably consistent with that of typical full-scale tidal turbine.

However, given the inherent challenges involved in subjecting a model rotor to realistic onset turbulence, several researchers have instead used surface waves in an attempt to investigate the hydrodynamic behaviour in an unsteady conditions. Galloway et al. [59] (see also [60]) reported on experiments of a 800 m diameter model tidal turbine perturbed by regular waves with an intrinsic frequency of 0.75 Hz and height of 0.8 m (approximately 1.6 m height full-scale) while towed with a carriage speed of 0.9 ms^{-1}. They observed that this forcing induced a cyclic shaft thrust that had a range of 37% of the mean. While their results provided a quantification of the unsteady thrust perturbation, inferring the loading on the individual blades is difficult. This is because the non-coherent loading imparted by the surface waves was effectively averaged out across all three blades.

Barltrop et al. [61] reported on experiments conducted with a 350 mm diameter tidal turbine in a towing tank subjected to surface waves, but importantly, provided measurements of the blade-root bending moments. Time histories were presented for intrinsic wave frequencies between 0.5 Hz and 1.0 Hz, at a wave height of 150 mm and a carriage speed of 1.0 ms^{-1}. At a rotational speed of 200 rpm, this forcing corresponds to reduced frequencies of between $k = \pi f c/\Omega r = 0.020$ and 0.048 at the spanwise location of $0.75R$. For the highest frequency case, the dynamic load amplitudes were found to be 50% and 100% of the mean in the out-of-plane and in-plane directions, respectively. For the low frequency surface waves, the bending moment response was found to compare reasonably well with a prediction using a quasi-steady numerical blade-element-momentum model with no acceleration effects included. However, for the higher frequency cases the amplitudes were of the order of twice that of the model predictions. This implies that the unsteady hydrodynamic contribution from waves for the low frequency cases was relatively small, but became more significant as the frequency was increased.

In order to achieve a controllable unsteady flow which is uniform over the rotor plane and can approximate a turbulent eddy forcing, it therefore appears to be most beneficial to oscillate the turbine axially in the flow. As the desired forcing kinematics are known exactly, the phases can be identified with greater confidence than by using surface waves or with a turbulent flow. As is highlighted by the ITTC guidelines [56], the ability to generate a harmonic forcing can also facilitate frequency-domain based studies. While there is no Froude–Krylov force (which is induced by

the pressure field from the surface wave), for a foil section with relatively low volume the effect is expected to be small. Such an approach was used in the investigations reported by Whelan et al. [62] and Whelan [11] for which the thrust of a 300 mm diameter twin-bladed rotor perturbed axially using a towing carriage in a flume was measured. In an extension of Whelan's work, the investigations by McNae [15] utilised the same facility and set-up, but acquired measurements of the out-of-plane bending moment for oscillatory forcing.

However, if oscillatory motion is combined with a mean velocity generated by the current in a flume, boundary layer effects and background turbulence can lead to non-uniformities in the flow unless the flume is extremely large and well-designed. Therefore, an attractive approach recommended in the ITTC guidelines [56] for generating an unsteady flow with the appropriate level of complexity to study unsteady rotor hydrodynamics is to superimpose an unsteady surging motion upon a steady forward speed in calm water in a towing tank. This methodology was employed in the test campaigns reported by Milne and co-workers [25,63,64] conducted at the Kelvin Hydrodynamics Laboratory towing tank. An uncertainty analysis presented by Milne et al. [63] following ITTC recommended procedures, also demonstrated that by using this approach the errors were sufficiently small to allow for the effects of hydrodynamic unsteadiness to be quantified relative to the loading for steady flow.

5.2. Implications of the low Reynolds number on foil performance and blockage

An additional important consideration for model-scale testing of tidal turbines is that the Reynolds number at the outer blade sections (which generally experience the greatest loading) is typically around only 1×10^5. This is approximately an order of magnitude smaller than is expected at full-scale [65]. Interestingly, Gauriera et al. [66] have recently conducted a bench-marking exercise comparing the performance of the same 0.7 m diameter model tidal turbine tested in different facilities. These included the Kelvin Hydrodynamics towing tank and the Ifremer flume used by Maganga et al. [57] and Mycek et al. [58]. The results of the study demonstrated that the maximum power coefficient increased by approximately 20% when the Reynolds number at $0.7R$ was increased from 9×10^4 to 1.9×10^5 and other parameters remained constant. As Lissaman [67], Shyy et al. [68] and Genc et al. [69] have discussed, at these relatively low Reynolds numbers the laminar boundary layer on a foil is susceptible to premature separation. This can give rise to separation bubbles which can significantly degrade the hydrodynamic performance relative to that expected at full-scale.

Numerical approaches to compute the hydrodynamic performance of foils with significant separation have proved difficult. Experimental data at low Reynolds numbers for relatively thick foils, such as those expected to be used for tidal turbines are also generally scarce. Wind tunnel data by Selig et al. [70] showed that while the two-dimensional lift slope remained linear with angle of attack at moderate angles of attack, the magnitude of the lift on the 21% thick NREL S823 foil could be reduced by approximately 10% and drag increased by 400%. Interestingly, at relatively low angles of attack the lift coefficient remained comparatively large and the drag increased significantly.

In order to provide more experimental data on thick foils at low Reynolds numbers, Milne [25] presented force and pressure measurements for the 24% thick S814 foil section from tests in a closed-section wind tunnel. This is the same foil profile that was employed in their turbine experiments in the towing tank, as well as by Barltrop et al. [61]. This wind tunnel investigation found quantitatively similar degradations in the lift and drag as reported by Selig et al. [70]. The pressure distributions across the chord indicated the existence of laminar separation bubbles, which extended over 50% of the chord at Reynolds numbers of 1×10^5 and affected the global pressure distribution. Interestingly, flow separation on the pressure surface of the foil at angles of attack of less than 4° was also observed. This separation is believed to explain the relatively high lift and drag exhibited by the foil as well as the S823 foil at similar low angles of attack. Therefore, separation on the pressure surface is likely to be a characteristic of thick foils at low Reynolds numbers.

While these low Reynolds number effects are important for steady flow tests of tidal turbines, they have important additional implications for the investigations of the unsteady hydrodynamics loads. In terms of the strategy employed to control the rotor speed, the sensitivity of the lift and drag to the Reynolds number implies that using constant speed (as employed in the studies reported by Milne and co-workers), where the Reynolds number is approximately constant, is more desirable as opposed to constant torque (as used by Whelan [11], for example). Moreover, the ITTC [56] also cites the additional advantages of employing constant speed as enabling the effects related to angular accelerations for the rotor to be removed and that the rotor to be brought up to full-speed prior to commencing each test. This allows for more measurement time when testing in a towing tank with finite run length.

These effects of the Reynolds number also emphasise the importance of establishing the steady loads using the equivalent set-up, turbine and flow speeds as used in an unsteady test, such that the unsteady hydrodynamic contribution can be isolated. In line with this, the Reynolds number sensitivity also introduces an additional uncertainty when attempting to use numerical models, such as the blade-element-momentum based method, which are inherently reliant on accurate foil data. While these models may be useful for estimating important parameters such as the angles of attack and induced flow, the uncertainties are likely to be too large for accurate quantification of the unsteady loads.

In addition to the effect of the Reynolds number, it is also poignant to consider the influence of blockage in model scale testing in controlled facilities. For the previous experimental tests cited in Section 5.1 the blockage typically varied between around 5% and 10%, based on the ratio of the cross-sectional area of the turbine to that of the unrestricted flow. While these blockage levels have previously been considered to be relatively low, based on the findings of the round robin study reported by Gauriera et al. [66], these levels are still likely to be sufficient to influence the loading on a turbine. In general, the literature on blockage for tidal turbines are scarce and the validity of existing corrections are questionable. Therefore, there remains a need for a greater understanding of the blockage phenomena, particularly if unsteady flow is to be considered and appropriate corrections are to be developed.

6. Insights into the unsteady hydrodynamic loading on tidal turbines

6.1. Quantification of the effect of flow unsteadiness

The flume tank experiments reported by Mycek et al. [58] demonstrated a distinct sensitivity of the thrust coefficient of a single horizontal-axis tidal turbine to the turbulence intensity in the flow. In particular, within the typical operational range of the turbine (tip-speed ratios between 3 and 7) the thrust coefficients of approximately $C_T = 0.80$ decreased by around 10% when the turbulence intensity was varied from $I_u = 0.03$ to 0.15. Furthermore, the standard deviations of the thrust coefficients were approximately 3 times larger at the higher turbulence intensity,

increasing in value from $\sigma_{C_T}=0.05$ to 0.15. Interestingly, an energy spike in the C_T spectrum which corresponded to the blade passing frequency (of 4.13 Hz) was pronounced at the low intensity condition but not at the higher intensity. This finding is consistent with the eddy slicing effect being relatively small at the higher intensities in the experiment. However, this result may be strongly related to the scales of turbulence across the rotor generated in the flume and may not be transferable all turbines.

The experimental study by Whelan [11] was the first to show that for a turbine whose velocity was perturbed about a relatively high tip-speed ratio at low frequencies of $k=0.02$, the combined hydrodynamic added inertia for tidal turbines was generally positive. This agrees qualitatively with the effects attributed to dynamic inflow and true added mass for a rotor oscillating in heave [10]. Whelan [11] also found that the loading in-phase with velocity and which included both steady and unsteady hydrodynamic contributions was significantly greater than that which appeared in-phase with acceleration. Whelan quantified the inertial contribution through a coefficient defined by $C_I=\{F_x\}_{\dot{u}}/\rho V\dot{u}$, where $\{F_x\}_{\dot{u}}$ is the component of the axial thrust that appeared in-phase with acceleration and V is the volume enclosed by the rotor, and found that C_I was typically less than 0.05.

The investigations by Milne and co-workers [25,63,64] achieved significantly higher reduced frequencies than those of Whelan [11], of up to $k=0.07$. For relatively high tip-speed ratios for which the boundary layer was believed to be predominately attached across the outer sections of the blades, a sensitivity to the frequency of the forcing was identifiable. This is demonstrated in Fig. 4 which shows the phase-averaged hysteresis loops of the normalised out-of-plane blade root bending moment response to frequencies between $f=0.40$ and 0.80 Hz. The clockwise direction of the response is indicative of the phase of the bending moment leading the velocity and the equivalent steady flow loading is also shown for comparison. The study provided the first quantification of the unsteady hydrodynamic loading relative to the steady loads. The amplitudes and the phases estimated by fitting a harmonic model to the approximately linear responses are presented in Fig. 5. The amplitudes, which are normalised by fitting a linear curve to the loading measured for steady flow are shown to increase from approximately 1.05 to 1.15 when the reduced frequency is increased from $k=0.02$ to 0.05. The corresponding phase-lead is relatively small and decreases with an increase in the frequency ratio from approximately $\Phi=4.5^\circ$ to 1.5°.

As previously stated, the unsteady hydrodynamic loading comprises circulatory and non-circulatory forcing contributions. The non-circulatory forcing is due to the added mass and is present when a body accelerates in a fluid. Provided that the boundary layer remains attached, the unsteady circulatory effects include dynamic inflow. Dynamic inflow is associated with the backflow that is induced by changes in the vorticity in the wake of the turbine. It takes a finite time for the vorticity to build up following a change in the loading at the rotor plane, leading to an overshoot in the loading [15]. Given that these unsteady phenomenon are both dependent on the acceleration, they are challenging to separate experimentally [11]. However, the investigations reported by Milne [25] and also Milne et al. [64] provided interesting new insights into the role of the underlying hydrodynamic phenomena and their respective contributions. By estimating the non-circulatory added-mass contribution theoretically, Milne et al. presented the ratio of the bending moment in-phase with acceleration to the bending moment due to the non-circulatory forcing. These ratios were approximately equal to

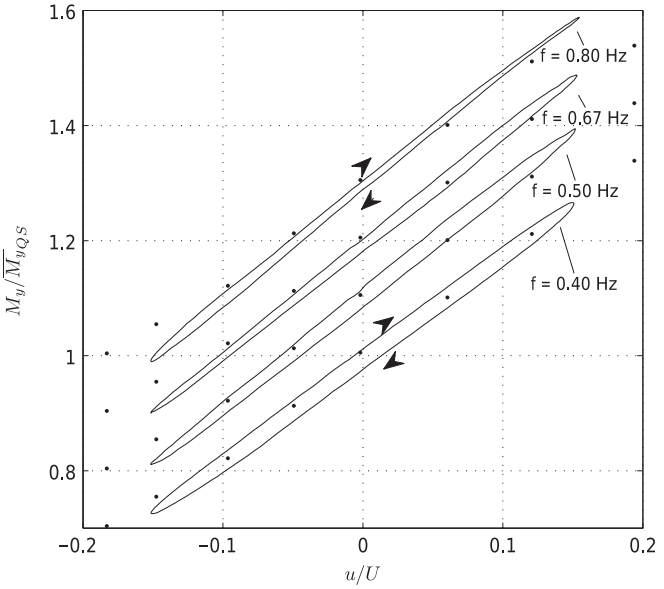

Fig. 4. The blade root out-of-plane bending moment for single frequency oscillations at a Current number of 0.150 demonstrating the effect of frequency, as presented by Milne [25]. The responses to the frequencies of $f=0.40$, 0.50, 0.67 and 0.80 Hz are consecutively offset upwards in intervals of 0.10 for clarity. The arrows indicate the direction of the phase of the response and the solid markers correspond to the bending moment measured for steady flow at the equivalent rotor speed and tip-speed ratio.

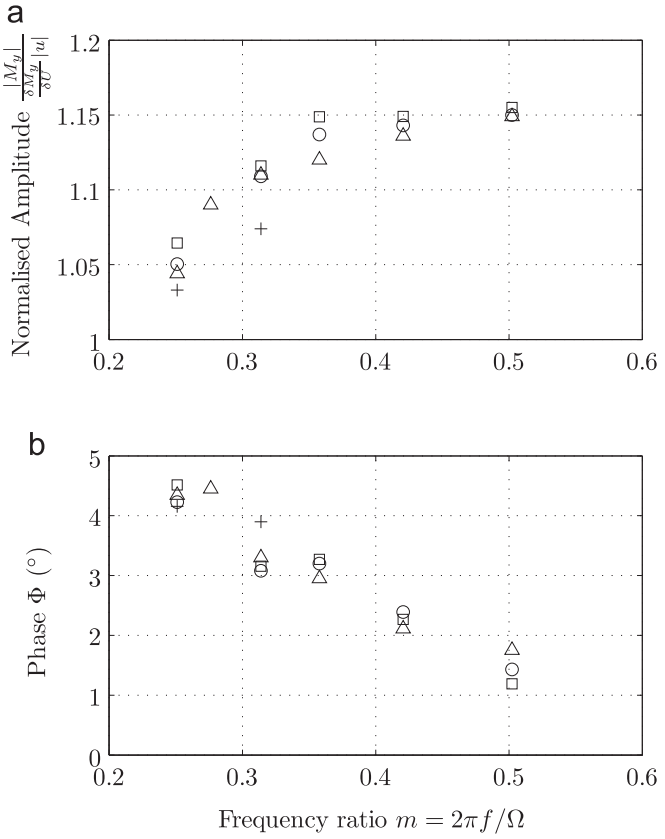

Fig. 5. Normalised amplitude (a) and phase-lead over velocity (b) of the blade root out-of-plane bending moment as a function of the frequency ratio and Current number (μ), as presented by Milne [25]. Legend: $\mu=$ 0.100 (□), 0.125 (○), 0.150 (△) and 0.175 (+).

2.7 at the lowest frequency and decreased with frequency ratio ($m = 2\pi f/\Omega$) to a value of 0.5 for m=0.5. A decrease in the circulatory forcing is consistent, qualitatively, with the induced velocity in the far wake being less able to respond to changes at the rotor plane at high frequencies (i.e. it tends towards the frozen wake state).

Finally, it is useful to consider the recent findings of McNae [15] who conducted a series of flume-based experiments which were a follow up to those by Whelan [11]. McNae presented bladeroot bending moment responses to oscillatory perturbations of the towing carriage where the rotor speed was not held constant. These showed that there was a small phase lag in bending moment response with respect to the oscillatory velocity at a frequency of 1 Hz (equivalent to a reduced frequency of k=0.025). The magnitude of the phase lag decreased for lower oscillatory frequencies and was approximately zero for the 0.2 Hz (k=0.005) case. The observation of a phase lag is in itself interesting, given that it is not commonly associated with dynamic inflow. However, the phase response was regarded to have been significantly influenced by the variable speed of the rotor and which lagged the oscillatory velocity during the experiment.

To better elucidate the role of the rotor speed, McNae [15] used a vortex lattice method to simulate the loading for an equivalent rotor geometry and velocity perturbations but with a constant rotational speed. These numerical results showed that the bending moment exhibited a relatively small phase lead over the velocity. Therefore, these responses are qualitatively consistent with the findings reported by Milne [25]. Furthermore, McNae [15] also used these simulations to show that the ratio between the velocity perturbation and the rotational frequency has an critical role on both the induced velocity and therefore the dynamic inflow effect. A higher frequency ratio can allow for greater roll up and therefore influence of the tip-vortices. These results again support the experimental findings of a sensitivity to the frequency ratio previously reported by Milne [25].

While these studies have shown that magnitude of the inertia component is relatively small compared to the total load, it should be recalled that the fluid and structural inertia are expected to be of the same order of magnitude [11]. This could be expected to have important implications on the design of the foundations of a turbine [15]. Furthermore, the added inertia is likely to be an important consideration in any control system for the rotor speed, particularly since the inertia contribution may vary significantly during operation.

6.2. Applications of oscillatory forcing responses

In Section 5.1 it alluded to that the generation of an unsteady forcing perturbation using a towing carriage could facilitate stochastic based analyses. Milne [25] (see also Milne et al. [64]) demonstrated this approach using a forcing which comprised a combination of the three oscillatory frequencies 0.40 Hz, 0.50 Hz and 0.67 Hz, each with a Current number of $\mu = 0.075$. An example of the time history for the blade root out-of-plane bending moment response is shown in Fig. 6(a). A small overshoot over the reconstruction based on the steady loading which is superimposed in grey is distinguishable.

The hysteresis loops for four relatively large fatigue inducing (see [41]) loading cycles corresponding to the responses between the symbols (○) and (●) on the time histories are shown in Fig. 6 (b). Milne [25] reconstructed the bending moment response using a linear superposition of the bending moment responses measured for the equivalent forcing and operating conditions for each of the individual single frequency oscillations. These reconstructions are shown in grey and comparisons between the true responses and the linear superposition-based responses reveal that by using this approach both the amplitude and phase of the multi-frequency responses are able to be replicated.

The ability to utilise the single frequency response in a transfer function-based approach to predict the amplitudes of the multi-frequency forcing is an attractive new finding. It implies that it could offer blade designers a relatively simple technique to obtain the fatigue loading from a turbulence spectrum. Furthermore, as Milne [25] also explored, the ability to recover the single frequency amplitudes (that are required to develop the amplitude part of the transfer function) from a multi-frequency forcing response by fitting a harmonic model is very useful. As experimental programmes are expensive and time-consuming, by using a multi-frequency forcing the testing could be completed in a relatively short time-frame, or conversely, a higher number of test-cases could be completed.

However, Milne [25] also demonstrated an important limitation of a linear superposition-based reconstruction for tidal turbines for combinations of relatively high frequencies. Consider the responses presented in Fig. 7 which correspond to a forcing that comprised the two oscillatory frequencies of f=0.67 and 0.80 Hz. Although the amplitude can be reconstructed using the single frequency responses, the phase (identifiable by the difference between the loading in the up-stroke and down-strokes parts of

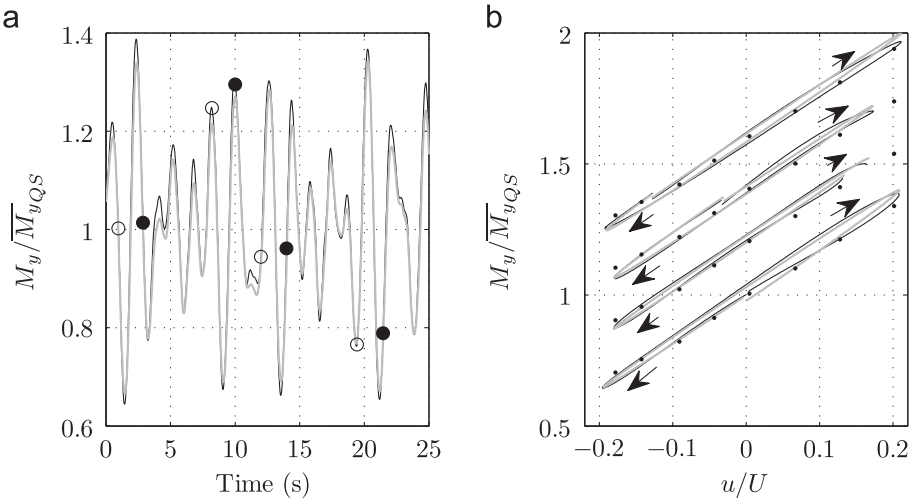

Fig. 6. Out-of-plane bending moment response to a forcing that comprised the frequencies $f = 0.40$ Hz, 0.50 Hz and 0.67 Hz, each with a Current number of $\mu = 0.075$, as presented by Milne [25]. In (a) the grey line is a reconstruction based on the steady flow load. In (b) the grey line is a reconstruction based on the linear superposition of the corresponding single frequency amplitudes and phases.

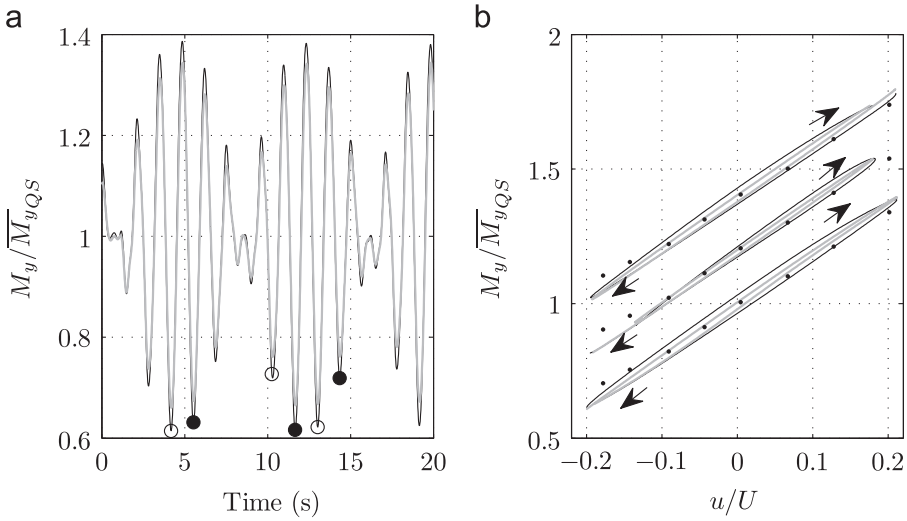

Fig. 7. Out-of-plane bending moment response to a forcing that comprised the frequencies $f = 0.67$ Hz and $f = 0.80$ Hz, each with a Current number of $\mu = 0.100$ [25]. The presentation of the data is consistent with Fig. 6.

the response) is larger than is able to be predicted using the single frequency responses. It is important to appreciate that the phase is driven by a physical phenomenon and cannot be averaged out. Therefore, this must be considered when utilising a stochastic approach to quantify the inertia loading on a turbine.

6.3. Hydrodynamic loading for separated boundary layer conditions

As stated previously, additional unsteady effects due to flow separation and dynamic stall on a rotor are present at relatively low tip-speed ratios (corresponding to high angles of attack). However, experimental studies which have specifically investigated the loading of tidal turbine blades (and also wind turbine blades) subjected to unsteady axial forcing under these operating conditions have been scarce.

Acknowledging the lack of data, Milne et al. [63] and also Milne [25] obtained the bending moment responses to axial oscillations of the rotor at two mean tip-speed ratios of $\lambda = 3.6$ and 4.1 corresponding approximately to maximum power. Examples of these responses for oscillatory frequencies of $f = 0.50$, 0.64, 0.89 and 1.40 Hz and a Current number of $\mu = 0.200$ are shown in Fig. 8. The hysteresis loops are presented by plotting the inverse of the instantaneous tip-speed ratio (i.e. $(U+u)/\Omega R$) on the abscissa and the total bending moment on the ordinate. The corresponding loads measured in steady flow are depicted by the dots.

While the cases for the higher mean tip-speed ratio of $\lambda =$ 4.1 exhibit similar trends to the responses for oscillations about $\lambda =$ 4.5 in Fig. 4 (particularly for low frequencies) the responses for $\lambda = 3.6$ with their much larger loops exhibit characteristics which are synonymous with the dynamic stall of oscillating foils; see Leishman [10]. For instance with an increase in the frequency the bending moment increasingly exceeds the maximum bending moment that is observed for the steady flow conditions, which is indicated by the region between the points 1 and 2 in Fig. 8. This is consistent with a delay in the onset and the progression of the trailing-edge separation on the boundary layer of the foils. At high instantaneous velocity, a vortex is likely to have reached the trailing edge and separated from the foil, resulting in lift stall which is indicated by point 3. Full separation of the boundary layer is attributed to the sudden and severe decrease in the bending moment and the subsequent pronounced non-linear hysteresis occurring between points 3 and 4. The boundary layer is able to re-establish on the surface of foil (point 5) as the angle of attack is reduced (i.e. as $1/\lambda$ has decreased). An increase in frequency can also be observed to have delayed the onset of flow reattachment to lower values of $1/\lambda$.

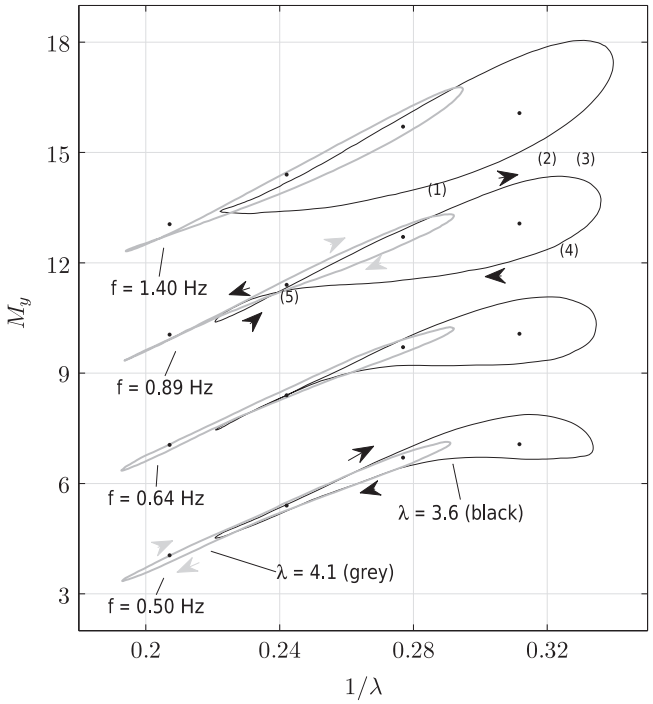

Fig. 8. Effect of the oscillatory frequency on the blade root out-of-plane bending moment response (Nm) for low mean tip-speed ratios of $\lambda = 3.6$ and $\lambda = 4.1$ (grey) at a rotor speed of 84 rpm and a Current number of $\mu = 0.200$ [25]. From bottom: $f = 0.50$ Hz, 0.64 Hz, 0.89 Hz, and 1.40 Hz, offset upwards in intervals of 3 Nm for clarity and presented as a function of the inverse of the instantaneous tip-speed ratio. The loads measured for steady flow are denoted by the solid markers and the out-of-plane response for f=0.89 Hz is annotated to correspond with the description of the underlying flow phenomena provided in Section 6.3.

These observations are of particular concern for tidal turbines which are stall regulated. They demonstrate that the magnitudes of the unsteady loads associated with separated flow are significantly larger (up to 10% from the data of Milne et al. [35]) than for an attached boundary layer. Furthermore, the highest frequency cases show that the reattachment occurs near the minimum oscillatory velocity. Therefore, the unsteady flow constituents can have a dominant role in the response over the entire load cycle.

7. Future directions

With the tidal energy industry continuing to develop, more measurements of turbulence in tidal flows with speeds of the order of $U = 2\ \mathrm{ms}^{-1}$ will become available. Such data will assist in establishing the variability in the turbulence among sites with more certainty. Of particular interest would be the acquisition of data which could reveal the spatial coherence of the streamwise velocity. This data cannot be obtained from a single 4-beam ADCP and likely necessitates an array of ADVs to be deployed. Sellar et al. [71] also demonstrated the possibility of using converging acoustic beams which could resolve the three-dimensional velocity vector at a focal point. It may be plausible to use a similar set up with a series of converging beams to resolve the velocity at multiple points across the rotor plane.

As the amplification of the turbulence due to the turbine is believed to be significant, measurements of turbulence in the presence of a full-scale turbine would be desirable. The experimental set up shown by Sellar et al. [71] included an acoustic beam which projected in a horizontal direction from the hub of the turbine. Although the velocities from this sensor were not presented, it is envisaged that a similar set up could potentially provide a means to measure the turbulent velocity at the rotor plane and at set intervals upstream. As such, the methodology could enable the theoretically-based estimates of the effect of amplification presented in Section 4.2 to be validated.

The recent model-scale experimental studies discussed in this review can now provide the tidal turbine industry with a valuable set of blade responses by which the validation of numerical models may be attempted. Milne [25] attempted to verify the dynamic inflow model of Peters (see Peters [72]) and a modified version of the returning wake model of Loewy [73] with the single frequency responses for high tip-speed ratios measured in their towing tank tests. While qualitative agreement was found at low frequencies, these also highlighted several shortcomings of the models which were originally devised for helicopter rotors in hover. In particular, these models do not account for the loss of circulation from the tips of the blade. It was shown by Goldstein [74] that for a rotor with a low number of blades and a low tip-speed ratio, such as a tidal turbine, the tip loss can affect over 40% of the blade. Therefore, vortex-wake models which better capture the circulation around the blade, such as that which was recently developed by McNae [15] for dynamic inflow studies, are likely to draw increasing attention.

For stall regulated turbines in particular, the unsteady, separation-induced loads will not be able to be predicted using the relatively simple transfer function or dynamic-inflow models given that they are non-linear. To account for delayed separation and dynamic stall, the semi-empirical model proposed by Leishman and Beddoes [75] has been adapted for rotors and incorporated into simulation codes for tidal turbines [76]. Initial attempts to verify the delayed stall component of this model by Milne [25] using the scale-model data, demonstrated qualitative agreement, but generally predicted flow re-attachment to occur too early. The model could only be assessed using the out-of-plane bending moment and substantial validation of the model still remains necessary to confidently assess its performance for tidal turbines. However, it is important to consider the limitations of the model. For instance, it was derived for thin foils oscillating in two-dimensional simple harmonic motion and is semi-empirical, requiring several foil-specific constants and high quality airfoil data. Given its shortcomings, more complex models are likely to be required for detailed design purposes.

While the primary objective of this review was to consider the turbulence-induced unsteady loads, it is important to consider that unsteady loading may be induced on a rotor that is misaligned to the flow, from surface waves and possibly from long period mooring oscillations in the case of floating installations. Furthermore, unsteady loads can arise from rapid changes in the pitch angle of the blades and which may affect the control strategies employed to regulate power. In particular, through full-scale wind turbine tests, it was found the unsteady loading of the blades associated with a rapid change in the pitch angle of a wind turbine to be more significant than that from a change in axial velocity [77]. The numerical studies presented by McNae [15] also came to similar conclusions for a tidal turbine. However, there appears to be scarce experimental studies which have verified this for tidal turbines. While a pitch actuator system may be technically challenging to achieve at model-scale, the experimental methodology used in the investigations by Whelan [11], McNae [15] and Milne [25] could be extended to investigate a non-zero yaw angle by tilting the rotor vertically, provided that the free-surface effects are kept small.

8. Conclusions

This paper has collated new experimental data and analyses that can assist designers of tidal turbines in quantifying the hydrodynamic blade loads due to onset turbulence.

Acoustic Doppler-based sensors have enabled the magnitudes and scales of turbulence of interest to be quantified in fast-flowing tidal streams. New evidence has been found to show that the near-bed turbulence structure at a tidal energy site is consistent with that expected for an open-channel flow. This has brought into question the use of atmospheric-based models for tidal turbine load predictions. Recent studies have also provided support for the hypothesis that the dominant eddies scale with elevation near the bed and begin to tend to isotropy at a near universal value of $k_x z = 3$–5. At typical hub heights, the turbulence intensity appears to be relatively consistent between sites at around 0.06–0.08. Relatively simple models also appear to be useful for predicting the magnitudes of the velocity fluctuations and the Reynolds stress.

These new observations of turbulence, together with theoretical analyses have demonstrated that owing to rotational sampling of turbulence, the reduced frequencies due to turbulence are between $k = 0.03$ and 0.10. The Current numbers could be as high as $\mu = 0.25$ due to the amplification of the turbulence by the presence of a turbine.

A variety of techniques developed by investigators have assisted in informing new best practices for testing tidal turbines in unsteady flow at model scale. The use of planar oscillatory forcing experiments in a still water towing tank have enabled the relative contribution of hydrodynamic unsteadiness on the blade-root bending moment to be quantified. For single frequency oscillations the unsteady blade loads have been shown to increase with frequency and exceed the steady loads by up to 15% as well as exhibit phase leads over velocity. This is consistent with the expected affects of dynamic inflow and non-circulatory forcing. Interestingly, the amplitudes of a multi-frequency forcing have been demonstrated to be able to be modelled using a linear superposition of the single frequency forcing response. Therefore, this potentially provides the blade designer with a relatively simple means of obtaining the fatigue loads by superposition.

Phenomena consistent with delayed separation and dynamic stall of oscillating foils have been observed in the blade load responses at low tip-speed ratios. These effects can result in a bending moment that exceeds the steady load by up to 25% and exhibits a large degree of hysteresis. Therefore, the unsteady hydrodynamic contribution from these effects can be more

significant than from the attached flow circulatory effects (dynamic inflow) or the non-circulatory forcing.

Acknowledgements

I.A. Milne wishes to acknowledge the New Zealand Tertiary Education Commission for funding his Ph.D. research through the Bright Futures Top Achiever Doctoral Scholarship. A.H Day also wishes to acknowledge support from UK EPSRC grant EP/F062036/1 “Feasibility of an Innovative Methodology for Testing Marine Current Turbines in Unsteady Flow”.

References

[1] GL. Rules for classification and construction, IV Industrial services, Part 14 – offshore wind energy, Guideline for the certification of ocean energy converters part 1 ocean current turbines; Germanischer Lloyd, 2005.
[2] Wolfram J. On assessing the reliability and availability of marine energy converters: the problems of a new technology. Proc Inst Mech Eng, Part O: J Risk Reliab 2006;220(1):55–68.
[3] Anyi M, Kirke B, Ali S. Remote community electrification in Sarawak. Malays Renew Energy 2010;35(7):1609–13.
[4] Liu P, Veitch B. Design and optimization for strength and integrity of tidal turbine rotor blades. Energy 2012;46(1):393–404.
[5] Marsh G. Wave and tidal power an emerging new market for composites. Reinf Plast 2009;53(5):20–4.
[6] Zhou F, Mahfuz H, Alsenas GM, Hanson HP. Static and fatigue analysis of composite turbine blades under random ocean current loading. Mar Technol Soc J 2013;47(2):59–69.
[7] Grant HL, Stewart RW, Moilliet A. Turbulence spectra from a tidal channel. J Fluid Mech 1962;12(02):241–68.
[8] McCaffrey K, Fox-Kemper B, Hamlington PE, Thomson J. Characterization of turbulence anisotropy, coherence, and intermittency at a prospective tidal energy site: observational data analysis. Renew Energy 2015;76(0):441–53.
[9] Peters DA, Boyd DD, He CJ. Finite-state induced-flow model for rotors in hover and forward flight. J Am Helicopter Soc 1989;34(4):5–17.
[10] Leishman JG. Principles of helicopter aerodynamics. 2nd ed. Cambridge Aerospace: Cambridge University Press; 2006.
[11] Whelan JI. A fluid dynamic study of free-surface proximity and inertia effects of tidal turbines [Ph.D. thesis]. Imperial College of Science, Technology and Medicine; 2010.
[12] Batten WMJ, Bahaj AS, Molland AF, Chaplin JR. Hydrodynamics of marine current turbines. Renew Energy 2006;31(2):249–56.
[13] Bahaj AS, Batten WMJ, McCann G. Experimental verifications of numerical predictions for the hydrodynamic performance of horizontal axis marine current turbines. Renew Energy 2007;32(15):2479–90.
[14] Fraenkel P. Windmills below the sea: a commercial reality soon?. Refocus 2004;5(2):46–8.
[15] McNae DM. Unsteady hydrodynamics of tidal stream turbines [Ph.D. thesis]. Imperial College, London; 2014.
[16] Kolmogorov AN. Local structure of turbulence in an incompressible fluid for very large Reynolds numbers. Dokl Acad Sci USSR 1941;31:301–5.
[17] Heathershaw AD. The turbulent structure of the bottom boundary layer in a tidal current. Geophys J Int 1979;58:395–430.
[18] Soulsby RL. Similarity scaling of turbulence spectra in marine and atmospheric boundary layers. J Phys Oceanogr 1977;7(6):934–7.
[19] Gross TF, Nowell AR. Spectral scaling in a tidal boundary layer. J Phys Oceanogr 1985;15:496–508.
[20] Townsend AA. The structure of turbulent shear flow. 2nd ed.. Cambridge: Cambridge University Press; 1976.
[21] Simpson J, Rippeth R, Williams E, Betteridge KFE. Marine turbulence: theories, observations, and models. In: Results of the CARTUM project, Acoustic doppler techniques. Cambridge University Press; Cambridge 2005. p. 127–38.
[22] Lohrmann A, Hackett B, Red LP. High resolution measurements of turbulence, velocity and stress using a pulse-to-pulse coherent sonar. J Atmos Ocean Technol 1990;7(1):19–37.
[23] Stacey MT, Monismith SG, Burau JR. Measurements of Reynolds stress profiles in unstratified tidal flow. J Geophys Res 1999;104(C5):10,933.
[24] Osalusi E, Side J, Harris R. Structure of turbulent flow in EMEC's tidal energy test site. Int Commun Heat Mass Transf 2009;36(5):422–31.
[25] Milne IA. An experimental investigation of turbulence and unsteady loading on tidal turbines [Ph.D. thesis]. The University of Auckland; 2014.
[26] Bouferrouk A, Hardwick JP, Colucci AM, Johanning L. Quantifying turbulence from field measurements at a mixed low tidal energy site. Renew Energy 2016;87:478–92 Part 1.
[27] Lu Y, Lueck R. Using a broadband ADCP in a tidal channel. Part II: Turbul J Atmos Ocean Technol 1999;16:1568–79.
[28] Atle L, Ramon C, Kraus NC. Acoustic-Doppler velocimeter (ADV) for laboratory use. In: Fundamentals and advancements in hydraulic measurements and experimentation proceedings. New York: ASCE; 1–5 August 1994. p. 351–65.
[29] Voulgaris G, Trowbridge JH. Evaluation of the acoustic Doppler velocimeter (ADV) for turbulence measurements. J Atmos Ocean Technol 1998;15(1):272–89.
[30] Kim S, Friedrichs C, Maa J, Wright L. Estimating bottom stress in tidal boundary layer from acoustic doppler velocimeter data. J Hydraul Eng 2000;126(6):399–406.
[31] Sherwood CR, Lacy JR, Voulgaris G. Shear velocity estimates on the inner shelf off Grays Harbor, Washington, USA. Cont Shelf Res 2006;26(1718):1995–2018.
[32] Trevethan M. A fundamental study of turbulence and turbulent mixing in a small subtropical estuary [Ph.D. thesis]. University of Queensland, Australia, September 2007.
[33] Walter RK, Nidzieko NJ, Monismith SG. Similarity scaling of turbulence spectra and cospectra in a shallow tidal flow. J Geophys Res 2011;116(C10019).
[34] Thomson J, Polagye B, Durgesh V, Richmond MC. Measurements of turbulence at two tidal energy sites in Puget Sound, WA. IEEE J Ocean Eng 2012;37(3):363–74.
[35] Milne IA, Sharma RN, Flay RGJ, Bickerton S. Characteristics of the turbulence in the flow at a tidal-stream power site. Philos Trans R Soc A: Math Phys Eng Sci 2013;371.
[36] McCann G, Thomson M, Hitchcock S. Implications of site-specific conditions on the prediction of loading and power performance of a tidal stream device. In: Proceedings of the 2nd International Conference on Ocean Energy, Brest, France; 2008.
[37] Milne IA, Sharma RN, Flay RGJ, Bickerton S. The role of onset turbulence on tidal turbine blade loads. In: Proceedings of the 17th Australasian fluid mechanics conference, Auckland, New Zealand, 5–9 December 2010.
[38] MacEnri J, Reed M, Thiringer T. Influence of tidal parameters on SeaGen flicker performance. Philos Trans R Soc Lond A: Math Phys Eng Sci 2013;371(1985) ISSN 1364-503X.
[39] Gunawan B, Neary VS, Colby J. Tidal energy site resource assessment in the East River tidal strait, near Roosevelt Island, New York, New York. Renew Energy, 71; 2014. p. 509–17. ISSN 0960-1481.
[40] Blumberg AF, Pritchard DW. Estimates of the transport through the east river, new york. J Geophys Res: Oceans 1997;102(C3):5685–703.
[41] Sutherland HJ. On the fatigue analysis of wind turbines. Technical Report SAND99-0089, Sandia National Laboratories; 1999.
[42] Osalusi E. Analysis of wave and current data in a tidal energy test site [Ph.D. thesis]. Heriot-Watt University, Institute of Petroleum Engineering; 2010.
[43] Lumley JL, Panofsky HA. The structure of atmospheric turbulence, vol. 12. New York: Wiley Interscience; 1964.
[44] Bradshaw P, Ferriss DH, Atwell NP. Calculation of boundary-layer development using the turbulent energy equation. J Fluid Mech 1967;28(03):593–616.
[45] Nezu I. Open-channel flow turbulence and its research prospect in the 21st century. J Hydraul Eng 2005;131(4):229–46.
[46] Nezu I, Nakagawa H. Turbulence in open-channel flows. A.A. Balkema, Rotterdam, 1993.
[47] Lien R-C, Sanford TB. Spectral characteristics of velocity and vorticity fluxes in an unstratified turbulent boundary layer. J Geophys Res 2000;105(C4):8659–72.
[48] Tennekes H, Lumley JL. A first course in turbulence. Cambridge, MA: MIT Press; 1972.
[49] Burton T, Sharpe D, Jenkins N, Bossanyi E. Wind energy handbook. Chippenham, UK: John Wiley and Sons; 2001.
[50] ESDU. Characteristics of atmospheric turbulence near the ground part II: single point data for strong winds (neutral atmosphere); ESDU 85020, Engineering Science Data Unit, London, 1974 (amended 1993).
[51] Connell JR. The spectrum of wind speed fluctuations encountered by a rotating blade of a wind energy conversion system. Sol Energy 1982;29(5):363–75.
[52] MCT. SeaGen technology, ⟨http://www.marineturbines.com/Seagen-Technology⟩; 2013 [accessed 08.01.13].
[53] Batchelor GK. The theory of homogeneous turbulence. Cambridge: Cambridge University Press; 1953.
[54] Graham JMR. Turbulent flow past a porous plate. J Fluid Mech 1976;73(03):565–91.
[55] McNae DM, Graham JMR. Effects of dynamic inflow and distortion of incident turbulence on tidal turbine rotors. In: Proceedings of the 3rd Oxford tidal energy workshop, 7–8 April 2014.
[56] ITTC. Model tests for current turbines. ITTC – recommended procedures and guidelines. 7.5-02-07-03.9; International Towing Tank Committee 2014.
[57] Maganga F, Germain G, King J, Pinon G, Rivoalen E. Experimental study to determine flow characteristic effects on marine current turbine behaviour. IET Renew Power Gener 2010;4(6):498–509.
[58] Mycek P, Gaurier B, Germain G, Pinon G, Rivoalen E. Experimental study of the turbulence intensity effects on marine current turbines behaviour. Part I: one single turbine. Renew Energy 2014;66(0):729–46 ISSN 0960-1481.
[59] Galloway PW, Myers LE, Bahaj AS. Studies of a scale tidal turbine in close proximity to waves. In: Proceedings of the 3rd international conference on ocean energy, Bilbao, Spain, 6–8 October 2010.
[60] Galloway PW, Myers LE, Bahaj AS. Quantifying wave and yaw effects on a scale tidal stream turbine. Renew Energy 2014;63:297–307.
[61] Barltrop N, Varyani KS, Grant A, Clelland D, Pham XP. Wave-current interactions in marine current turbines. Proc Inst Mech Eng – Part M – J Eng Marit Environ 2006;220(4):195–203.

[62] Whelan JI, Graham JMR, Piero J. A free-surface and blockage correction for tidal turbines. J Fluid Mech 2009;624(1):281–91.
[63] Milne IA, Day AH, Sharma RN, Flay RGJ. Blade loads on tidal turbines in planar oscillatory flow. Ocean Eng 2013;60C:163–74.
[64] Milne IA, Day AH, Sharma RN, Flay RGJ. Blade loading on tidal turbines for uniform unsteady flow. Renew Energy 2015;77:338–50.
[65] Myers L, Bahaj AS. Simulated electrical power potential harnessed by marine current turbine arrays in the Alderney Race. Renew Energy 2005;30(11):1713–31.
[66] Gaurier B, Germain G, Facq JV, Johnstone CM, Grant AD, Day AH, Nixon E, Di Felice F, Costanzo M. Tidal energy "Round Robin" tests comparisons between towing tank and circulating tank results. Int J Mar Energy 2015;12:87–109.
[67] Lissaman PBS. Low-Reynolds-number airfoils. Ann Rev Fluid Mech 1983;15:223–39.
[68] Shyy W, Lian Y, Tang J, Viieru D, Liu H. Aerodynamics of low Reynolds number flyers, 22. Cambridge University Press; 2008.
[69] Genç MS, Karasu İ, Açıkel HH, Akpolat MT. Low Reynolds number aerodynamics and transition, in: Low Reynolds number flows and transition; 2012. p. 162. InTech.
[70] Selig MS, Guglielmo JJ, Broeren AP, Gigure P. Summary of low-speed airfoil data, 1. Virginia Beach, VA, USA: SoarTech Publications; 1995.
[71] Sellar B, Harding S, Richmond M. High-resolution velocimetry in energetic tidal currents using a convergent-beam acoustic Doppler profiler. Meas Sci Technol 2015;26(8).
[72] Peters DA. How dynamic inflow survives in the competitive world of rotor aerodynamics. J Am Helicopter Soc 2009;54(1):1–15.
[73] Loewy RG. A two-dimensional approximation to the unsteady aerodynamics of rotary wings. J Am Helicopter Soc 1957;24(2):81–92.
[74] Goldstein S. On the vortex theory of screw propellers. Proc R Soc Lond Ser A 1929;123(792):440–65.
[75] Leishman JG, Beddoes TS. A semi-empirical model for dynamic stall. J Am Helicopter Soc 1989;34(3):3–17.
[76] Bossanyi EA. GH tidal bladed theory manual. Bristol, UK: Garrad Hassan and Partners; 2009.
[77] Snel JG, Schepers H. Joint investigation of dynamic inflow effects and implementation of an engineering method. Technical Report ECN-94-104; 1995.